Supplementary Information

Large anomalous Hall effect and negative magnetoresistance in half-topological semimetals

Yanglin Zhu[1,2+], Cheng-Yi Huang[3+], Yu Wang[1], David Graf [4], Hsin Lin[5], Seng Huat Lee[1], John Singleton[6], Lujin Min[1], Johanna C. Palmstrom[6], Arun Bansil[3], Bahadur Singh[7*], and Zhiqiang Mao[1*]

[1] Department of Physics, Pennsylvania State University, University Park, PA, USA, 16802

[2] School of Physics and Technology, Nanjing Normal University, Nanjing, China, 210046

[3] Department of Physics, Northeastern University, Boston, USA, 02115

[4] National High Magnetic Field Laboratory, Tallahassee, FL, USA, 32310

[5] Institute of Physics, Academia Sinica, Taipei 11529, Taiwan

[6] National High Magnetic Field Laboratory, Pulsed Field Facility, Los Alamos National Laboratory, Los Alamos, NM, USA, 87545

[7] Department of Condensed Matter Physics and Materials Science, Tata Institute of Fundamental Research, Mumbai 400005, India

Supplementary Note 1: High temperature Hall resistivity data

Besides the Hall resistivity measured under high magnetic fields (up to 31T) at ≤ 20K presented in the main text (Fig. 1a), we also measured the Hall resistivity of our sample at high temperatures (up to 200K) using a PPMS with a 9T magnet. Although we conducted measurements only up to 9T at high temperatures, the anomalous Hall resistivity (AHE) peak is still observable at 30K and 50K but vanishes above 100K (Fig. S2c below). Note that the field dependence of normal Hall resistivity at high temperatures significantly differs from that at low temperatures. As discussed in the main text, the normal Hall resistivity at low temperatures (<10K) exhibited a linear field dependence with a positive slope at fields above 15T (Fig. 1a in the main text), indicating that holes are the major carriers. However, at high temperatures, thermal effects lead to the presence of excited electrons, so that both electrons and holes will contribute to transport and the field dependence of normal Hall resistivity will not be linear. The Hall resistivity data at 100 K and 200 K indeed show multi-band features. The data of 200K can be fitted quite well by a two-band model as shown by the dashed curves in Fig. S2c, while the fit for the data at 100K shows clear deviations. The Hall resistivity data below 50K cannot be fitted at all with the two-band model. These results indicate that the AHE peak becomes weak above 50K. Transport involving contributions from multiple bands at higher temperatures is also evidenced by the temperature dependence of resistivity ρ_{xx} of TbPdBi shown Fig. S1a, which exhibits a broad peak around 50K. The semiconducting-like behavior above 50K clearly shows that high temperature transport is dominated by excited charge carriers.

In order to further verify the above interpretation, we measured another TbPdBi sample up to 18T and 100K using the same field and current configuration shown in Fig. 1a [**I**//(100) and **B** ⊥ (100)]. The data obtained on this sample (supplementary Fig. S2d) is consistent with the above interpretation. The two-band model fit is very good even at 100K but it breaks down below 50K due to the presence of the AHE peak. The samples used in these two measurements may differ slightly in their chemical potentials.

Although the AHE peaks at 10-20K (Figs. 1a and S2d) are higher than those at temperatures below T_N, there exist some multiple-band normal Hall contributions. As discussed in the main text, the normal Hall contribution due to thermal excitations could lead to multiple-band effects in Hall resistivity, which could result in a broad normal Hall resistivity peak overlapping with the AHE peak. The broad peaks seen at 30K and 50K (supplementary Fig. S2c) are most likely dominated by multiple-band normal Hall contributions. In other words, the increase of the ρ_{xy} peak above T_N should arise from normal Hall contributions from multiple bands. This interpretation is supported by the following observations. At temperatures below T_N (e.g. 1.7 K and 4.0 K), the AHE peak remains sharp and hardly changes with temperature; its normal Hall contribution can be described by a single band scenario, as manifested by the linear field dependence of ρ_{xy} above 15 T below T_N. However, when the temperature is well above T_N (10 -20 K), the ρ_{xy} peak involves contributions not only from the AHE but also from multiple-band normal Hall effect, which is manifested by the clear deviation from the nonlinear field dependence of ρ_{xy} in the high-field limit. Nevertheless, it is hard to separate the anomalous Hall resistivity from the multiple-band normal Hall contribution for $T > T_N$.

Supplementary Note 2: Details of the anomalous Hall resistivity $\Delta\rho_{xy}^{AH}$ data analysis in the AFM state

TbPdBi undergoes an AFM-to-FM transition around 15T below T_N. Our DFT calculations indicate that this magnetic transition comes with an electronic structure transition. As shown in Figs. 3e and 3f in the main text, in the AFM state, TbPdBi is a semimetal with band inversion in both the spin channels and the bands crossing the Fermi level being hardly spin polarized. In contrast, as the AFM state is driven to a FM state by magnetic fields above 15T, the system evolves into a half-topological semimetal state with a single-spin-channel band inversion; that is, the spin-down bands cross the Fermi level, while the spin-up bands are pushed away from the Fermi level. In other words, the AFM-to-FM transition leads to a half-topological semimetal (HTS) state with high spin polarization. Such an electronic structure transition driven by the magnetic transition can be expected to lead to changes in carrier concentration.

In the FM phase above 15T for $T < T_N$, the Hall resistivity ρ_{xy} exhibits a linear field dependence (Fig. 1a), which can be attributed to normal Hall contributions. From the slope of ρ_{xy} above 15T in the FM phase at 4K, the carrier density is estimated to be ~ 5.19×10^{19} cm^{-3}. However, in the canted

AFM state below 15T, the anomalous Hall resistivity is mixed with the normal Hall resistivity and varies with magnetic field. Since there is an electronic structure transition involved in the AFM-to-FM transition, the normal Hall contribution should change across the magnetic transition. Although we can separate the normal Hall resistivity ρ_{xy}^{N} from the anomalous Hall resistivity $\Delta\rho_{xy}^{\mathrm{AH}}$ for the FM phase, where ρ_{xy}^{N} is linearly proportional to the field and $\Delta\rho_{xy}^{\mathrm{AH}}$ remains constant, we cannot separate ρ_{xy}^{N} from $\Delta\rho_{xy}^{\mathrm{AH}}$ for the canted AFM phase since $\Delta\rho_{xy}^{\mathrm{AH}}$ varies with magnetic field. In our analyses of $\Delta\rho_{xy}^{\mathrm{AH}}$ (supplementary Fig. S2a), we approximately assumed that the normal Hall resistivity ρ_{xy}^{N} in the canted AFM state follows the same linear field dependence as the FM phase (black dashed line in Fig. 1a). From the calculated band structures for both the AFM (Fig. 3f) and FM (Fig. 3e) states, the carrier density in the AFM phase should be lower than that in the FM phase since the FM phase has larger Fermi pockets. This implies that our extracted $\Delta\rho_{xy}^{\mathrm{AH}}$ is slightly underestimated so that the anomalous Hall angle of TbPdBi shown in Fig. 1d is also slightly underestimated.

Supplementary Note 3: Scaling behavior of the anomalous Hall conductivity

The large AHE observed in TbPdBi should be of intrinsic origin for the following reasons: i) The intrinsic anomalous Hall conductivity (AHC) can be much larger than the extrinsic AHC in some cases. As far as we know, the anomalous Hall angles due to the extrinsic AHE usually fall in the range of 0.1-1% [1], which is two orders of magnitude smaller than in TbPdBi. ii) The intrinsic and extrinsic origins of AHE can also be distinguished via the scaling behavior of the AHE. The intrinsic anomalous Hall conductivity $\sigma_{yx}^{\mathrm{AH}}$ is independent of the longitudinal conductivity σ_{xx} for moderately clean systems, while it is proportional to $\sigma_{xx}^{1.6}$ for multiband disordered metals[2]. In contrast, the extrinsic AHC $\sigma_{yx}^{\mathrm{AH}}$ in the clean region is proportional to σ_{xx}. To ascertain whether the AHE of TbPdBi is dominated by intrinsic or extrinsic effects, we plot the anomalous Hall conductivity $\sigma_{yx}^{\mathrm{AH}}$ (obtained via tensor conversion from the anomalous Hall resistivity and longitudinal Hall resistivity) as a function of the longitudinal conductivity σ_{xx} on a semilog scale in Fig. S6. The data is seen to be fitted by $\sigma_{yx}^{\mathrm{AH}} \propto \sigma_{xx}^{\alpha}$ with $\alpha = 0.6$. The σ_{xx} value of TbPdBi is within the range of 600-750 $\Omega^{-1}\mathrm{cm}^{-1}$, indicating that our sample is near the boundary between the disordered metal and the moderately clean regimes. As such, the scaling behavior of $\sigma_{yx}^{\mathrm{AH}} \propto \sigma_{xx}^{0.6}$ seen in TbPdBi should be attributed to the intrinsic origin. We thus conclude that even if an extrinsic AHE is present in TbPdBi, it does not have a dominant contribution.

Supplementary Note 4: Anisotropic behavior of the calculated anomalous Hall conductivity

The anisotropic behavior of the calculated anomalous Hall conductivity (AHC) in TbPdBi results from the magnetization in the spin-canted state in the presence of an external magnetic field, assumed here to be along the [100] direction. The intrinsic AHC solely depends on the band structure, and it is given by:

$$\sigma_{ij} = -e^2\hbar \int_{Bz} \frac{d^3k}{8\pi^3} \Omega_{ij}(\mathbf{k}).$$

Here, $\Omega_{ij}(\mathbf{k})$ represents the Brillouin zone (BZ) integral of the k-dependent Berry curvature tensor Ω. The Berry curvature tensor Ω exhibits the spin-symmetry of the crystal lattice in magnetic materials instead of the lattice symmetry. Therefore, even though the crystalline structure does not change in TbPdBi, its magnetic symmetry is lower than the cubic symmetry. In TbPdBi, while initially it displayed the antiferromagnetic (AFM) ground state, the application of an external magnetic field induces a transition into a spin-canted state. Within this state, magnetization M_s exerts a pronounced influence on the corresponding intrinsic Hall conductivity components. In the AFM state, the preserved C3 rotational symmetry about the [111] direction necessitates that $\sigma_{xy} = \sigma_{yz} = \sigma_{zx} = 0$ due to Berry curvature cancellation. It is noteworthy that for the [100] direction, the preserved symmetry is denoted as $\bar{S}_4$. In accordance with such symmetry, the AHC conforms to the relationships $\sigma_{xy} = \sigma_{xz} = \sigma_{x-y} = -\sigma_{xy}$, implying that $\sigma_{xy} = \sigma_{xz} = 0$. Also, $\sigma_{yz} = \sigma_{z-y} = -\sigma_{zy}$, which suggests σ_{yz} could be nonzero. However, initial AFM state where the magnetization M_s is zero (x =0 of Figure 4), $\sigma_{yz} = 0$ as well. After applying an external magnetic field along the [100] direction, the system transitions into a spin-canted state (0<x<1in Figure 4). In such a state, no symmetries are preserved, leading to the emergence of the net Berry curvature Ω_{yz} , and consequently, σ_{yz} exhibits a significant increase, as depicted in Figure 4. Our results are consistent with previous studies in various magnetic materials, such as bcc Fe [3], fcc Ni [4], hcp Co [5], and L10 FePt, CoPt, and NiPt ferromagnets [6], where the AHC strongly depend on the magnetization directions of the materials.

From an experimental perspective, we initially denote the field direction as the [100] direction (referred to x direction in theoretical calculations), resulting in the observed magnetization, denoted as M_{100}. Incorporating M_{100} into theoretical calculations yielded a nonzero Hall conductivity represented as σ_{yz}. Conversely, if we modify the field direction notation to [001] (termed as "z" in theoretical calculations), the nonzero AHC would manifest as σ_{xy}, so that the AHC within the plane perpendicular to the field direction experiences a significant anisotropy.

Supplementary Figure S1 | (a) Left axis: Temperature dependence of resistivity of TbPdBi. Right axis: magnetic susceptibility measured with **B** = 0.1T(**B**// [100]). Inset: AFM transition in resistivity and magnetic susceptibility. (b) Curie-Weiss fit to the inverse magnetic susceptibility of TbPdBi measured with **B** = 0.1T. (c) X-ray diffraction pattern for our TbPdBi crystal. The inset gives image of a typical crystal.

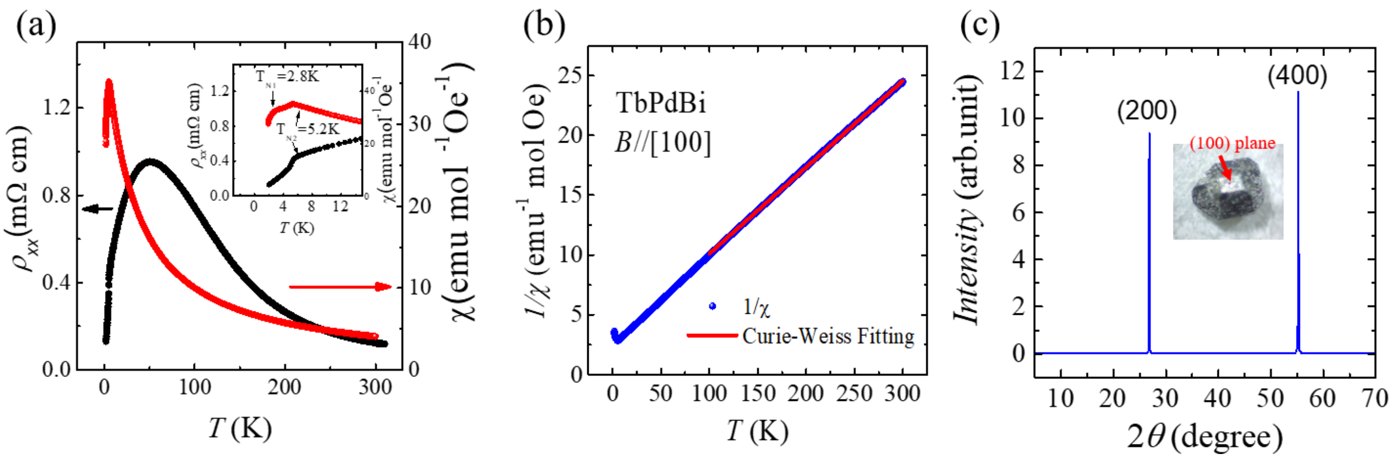

Supplementary Figure S2 | (a) Plot of $\Delta\rho_{xy}^{\mathrm{AH}}$ as a function of the magnetic field **B**. (b) Plot of the anomalous Hall conductivity (AHC) $\sigma_{yx}^{\mathrm{AH}}$ of TbPdBi as a function of the magnetic field B. (c) The Hall resistivity ρ_{xy} measured up to 200K using PPMS. (d) The Hall resistivity ρ_{xy} measured up to 100K and 18T for another TbPdBi sample.

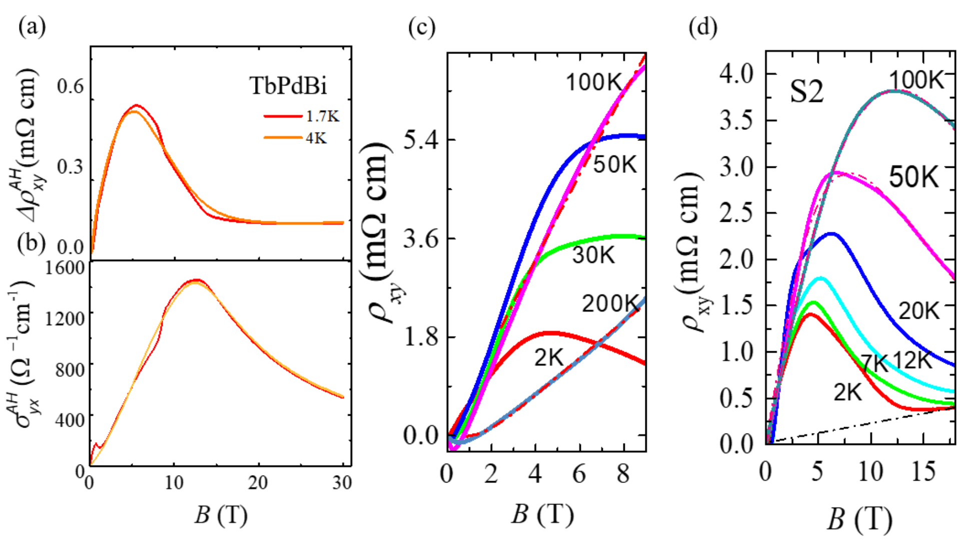

Supplementary Figure S3 | Raw longitudinal resistivity ρ_{xx} and Hall resistivity ρ_{xy} for TbPdBi measured at T=4K.

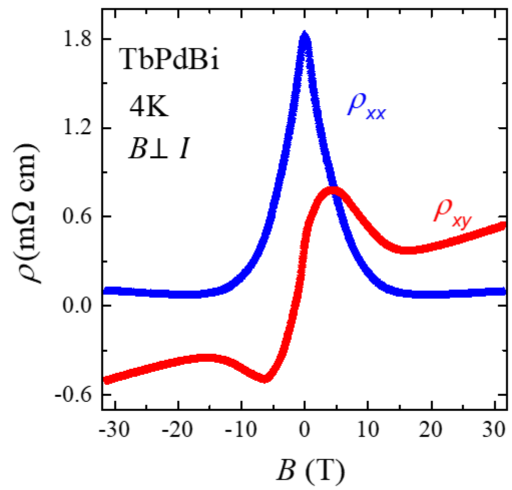

Supplementary Figure S4 | Plot of $\Delta\rho_{xy}^{\mathrm{AH}} = \rho_{xy} - R_0\mathbf{B}$, as a function of the isothermal magnetization M of TbPdBi.

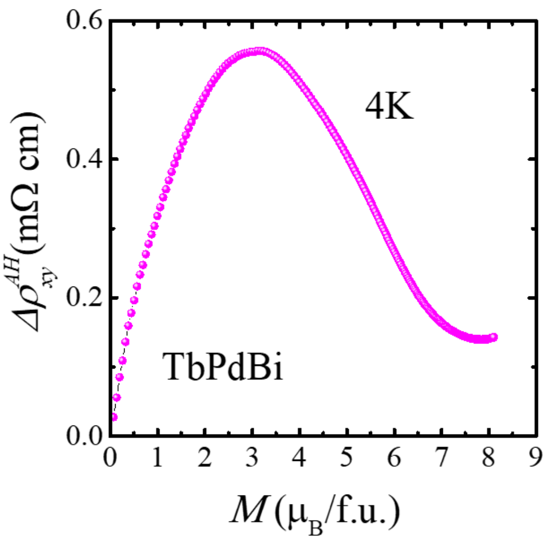

Supplementary Figure S5 | MR of TbPdBi at 1.7K: Field dependence of the longitudinal (black line) and transverse (red line) MR at 1.7K up to 31T. Inset shows the MR data at low fields.

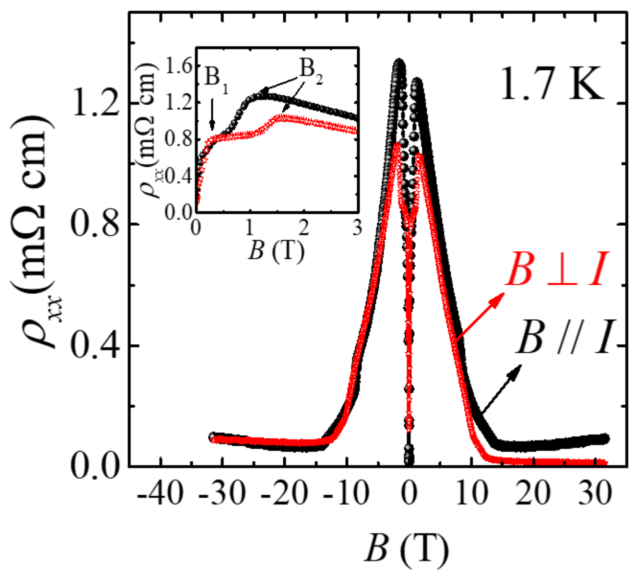

Supplementary Figure S6 | Anomalous Hall conductivity σ_{yx}^{AHE} as a function of the longitudinal conductivity σ_{xx} for TbPdBi.

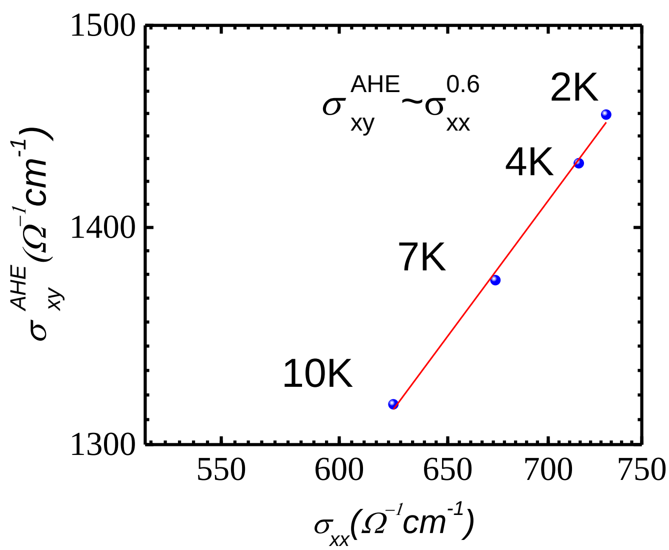

Supplementary Table I: Weyl nodes in the [100] FM state. *C* denotes chiral charge at Weyl nodes.

Label	k_x(Å^{-1})	k_y(Å^{-1})	k_z(Å^{-1})	E(eV)	C
1	0.070133	0.004677	-0.047861	0.076	+1
2	0.070510	-0.006450	0.049105	0.076	+1
3	-0.070395	0.046424	0.006932	0.073	-1
4	-0.070950	-0.048597	-0.006806	0.074	-1

Supplemenatary References:

[1] K. Wang, Y. Zhang, S. Zhou, and G. Xiao, Micron-Scale Anomalous Hall Sensors Based on FexPt1−x Thin Films with a Large Hall Angle and near the Spin-Reorientation Transition, Nanomaterials **11**, 4 (2021).

[2] W. R. Branford, K. A. Yates, E. Barkhoudarov, J. D. Moore, K. Morrison, F. Magnus, Y. Miyoshi, P. M. Sousa, O. Conde, A. J. Silvestre, and L. F. Cohen, Coexistence of Universal and Topological Anomalous Hall Effects in Metal CrO_2 Thin Films in the Dirty Limit, Physical Review Letters **102** 22, 227201 (2009).

[3] A. A. Hirsch and Y. Weissman, Anisotropy of the Hall effect in iron, Physics Letters A **44** 4, 239 (1973).

[4] G. V. F. N. V. Volkenshtein, and V. P. Shirokovskii, Sov. Phys. JETP **11**, 48 (1960).

[5] E. Roman, Y. Mokrousov, and I. Souza, Orientation Dependence of the Intrinsic Anomalous Hall Effect in hcp Cobalt, Physical Review Letters **103** 9, 097203 (2009).

[6] H. Zhang, S. Blügel, and Y. Mokrousov, Anisotropic intrinsic anomalous Hall effect in ordered 3dPt alloys, Phys. Rev. B **84** 2, 024401 (2011).